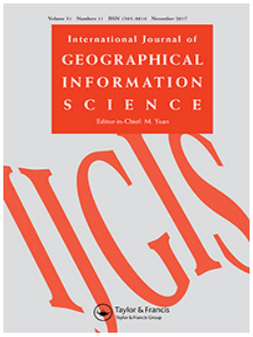

International Journal of Geographical Information Science

ISSN: 1365-8816 (Print) 1362-3087 (Online) Journal homepage: https://www.tandfonline.com/loi/tgis20

Reducing the grid orientation dependence of flow routing on square-grid digital elevation models

Jari Hyväluoma

To cite this article: Jari Hyväluoma (2017) Reducing the grid orientation dependence of flow routing on square-grid digital elevation models, International Journal of Geographical Information Science, 31:11, 2272-2285, DOI: 10.1080/13658816.2017.1358365

To link to this article: https://doi.org/10.1080/13658816.2017.1358365

Published online: 31 Jul 2017.

INTERNATIONAL JOURNAL OF GEOGRAPHICAL INFORMATION SCIENCE, 2017
VOL. 31, NO. 11, 2272–2285
https://doi.org/10.1080/13658816.2017.1358365

Taylor & Francis
Taylor & Francis Group

RESEARCH ARTICLES

OPEN ACCESS Check for updates

Reducing the grid orientation dependence of flow routing on square-grid digital elevation models

Jari Hyväluoma

Natural Resources Institute Finland (Luke), Jokioinen, Finland

ABSTRACT

Topographical parameters derived from digital elevation models by employing flow routing algorithms may depend on the orientation of the square grid. Grid orientation dependence results from the insufficient isotropy of square grid and affects the flow directions and subsequent calculations based on flow routing. In this article, a systematic approach for analysing the rotational invariance of flow accumulation calculations is presented and applied. Computed flow accumulation maps are found to depend strongly on the grid orientation, especially if flow routing methods with low dispersion are used. It is also shown that isotropy of flow routing algorithms can be significantly improved by introducing a numerical parameter resulting in adjustable weighting for cardinal and diagonal directions in flow routing. The actual value of this parameter depends on the used flow routing method.

ARTICLE HISTORY
Received 13 January 2017
Accepted 18 July 2017

KEYWORDS
Flow distribution; digital elevation model; rotational invariance; isotropy; grid orientation

1. Introduction

Surface topography is an important factor in hydrological modelling, erosion prediction and many environmental applications. In geographical information science (GIS), terrain surfaces are described by digital elevation models (DEMs) (Hengl and Reuter 2008). The most widely used format for terrain data in GIS is square-grid DEM, which can be stored in simple data structures and analysed with simple computational algorithms. Grid-based DEM is a discrete approximation of the real continuous terrain. In addition to actual precision of elevation data, computations relying on grid-based DEMs also display inaccuracies related to the finite grid spacing as well as orientation of the grid (see, e.g., Wolock and Price 1994, Zhou and Liu 2004, Sørensen and Seibert 2007).

Flow routing algorithms are utilized in calculation of directions and distribution of water flow over terrains described by DEMs. These calculations are needed in determination of flow accumulation and drainage network delineation, and further in, e.g., computation of so-called slope length and steepness (LS) factor in universal soil loss equation (USLE)-type erosion models (Kinnell 2010) or topographic wetness index (Beven and Kirkby 1979). Flow routing algorithms can be roughly divided into two classes, i.e. single-flow direction (SFD) (e.g. O'Callaghan and Mark 1984, Fairfield and Leymarie 1991, Lea 1994) and multiple-flow direction (MFD) (e.g. Freeman 1991, Quinn

CONTACT Jari Hyväluoma jari.hyvaluoma@luke.fi

et al. 1991, Costa-Cabral and Burges 1994, Holmgren 1994, Tarboton 1997, Qin *et al*. 2007) algorithms (for a review, see Wilson *et al*. 2008). In SFD algorithms, all water arriving to a grid cell is directed to exactly one neighbouring downslope grid cell. In MFD algorithms, the water in a cell can drain into several downslope cells. The choice of algorithm is always a compromise. While MFD algorithms are able to describe divergent flows, SFD algorithms are not. On the other hand, MFD methods exaggerate the flow dispersion (Tarboton 1997, Wilson 2012). Accuracy of different algorithms also depends on the terrain properties (Wilson *et al*. 2007, Qin *et al*. 2013).

Algorithms which process the elevation data given by grid DEMs can produce visual and numerical error patterns which reflect insufficient isotropy of the underlying square grid. Grid orientation thus affects flow directions (Fairfield and Leymarie 1991) and further calculations utilizing flow routing algorithms. For example, Zhou and Liu (2004) analysed and tested the impact of grid orientation on the slope and aspect values by using artificial DEMs. All algorithms tested in their work showed extreme values when grid was rotated multiples of 45° demonstrating so-called octant bias. Similar artefacts for flow accumulation patterns were observed already a quarter of a century ago by Freeman (1991). Since these uncertainties arise from insufficient symmetry of the computational grid, they cannot be removed by grid refinement.

Zhou and Liu (2002) identified three major error sources for topographical parameters derived from grid DEMs: (1) data accuracy of DEM itself; (2) spatial data structure of DEM including data precision, grid resolution and grid orientation; and (3) the employed mathematical models and algorithms. In this work, we concentrate on the errors arising from grid orientation, which belongs to the second error class in the classification of Zhou and Liu (2002).

Virtually all DEMs contain some artefacts. High-resolution LIDAR (light detection and ranging)-based DEMs often contain large number of small depressions. Flow directions cannot be accurately calculated before DEM is made 'hydrologically correct' by removing depressions and flat areas (see, e.g., Jenson and Domingue 1988, Garbrecht and Martz 1997, Grimaldi *et al*. 2007, Nardi *et al*. 2008). In this work, it is presumed that the handling of depressions and flat areas is performed as a preprocessing step.

Grid orientation dependence could be reduced by using hexagonal grids which have higher symmetry and thus better isotropy than square grids (de Sousa *et al*. 2006). Transition from square grids to hexagonal grids was crucial, e.g., in the development of lattice gas cellular automata. Hexagonal cellular automata with higher symmetry were able reproduce the fluid flow equations, which was not possible for square lattices (Frisch *et al*. 1986). Even though use of hexagonal grids could probably lead to more general solution to the present problem, it is likely that square grids will remain the most used data structure for DEMs and DEM-based computations. Therefore, in this article, we seek for solution that could reduce the grid orientation dependence of flow-routing-based computations relying on square-grid DEMs.

In this article, we investigate how square-grid format used for DEM data affects the results of DEM-based analyses relying on flow routing. As an example flow accumulation is considered, but the obtained results are expected to be exploitable also for other parameters relying on flow routing calculations. We use a power-law-form MFD algorithm (Freeman 1991, Holmgren 1994), which allows control over the numerical dispersion in the model. Our results show that rotational invariance of the algorithm weakens

with reducing dispersion. We also show that situation can be improved by introducing an additional parameter resulting in different and adjustable weighting for diagonal and cardinal directions in flow routing.

2. Methods and materials

2.1. *Flow routing*

Flow routing algorithms are employed when determining distribution of the overland flow over landscapes described by DEMs. Flow routing defines how water arriving a given grid cell is distributed to the eight nearest neighbour grid cells. Several algorithms that operate on square-grid DEMs have been developed (Wilson *et al*. 2008).

Simplest approach for flow routing is the D8 SFD algorithm (O'Callaghan and Mark 1984). D8 algorithm directs the water from a given grid cell to exactly one neighbouring grid cell. The destination cell is determined by calculating slope to each eight neighbouring cells and selecting the neighbouring cell with steepest downward slope.

Another popular approach is the FD8 MFD algorithm developed by Quinn *et al*. (1991). FD8 algorithm distributes the flow from a grid cell to all neighbouring downslope cells. Flow is apportioned to the destination cells on the basis of slope gradients.

FD8 algorithm has been further modified by using a power-law form in the calculation of flow fractions (Freeman 1991, Holmgren 1994). In this method, the flow fraction towards the neighbouring cell i ($i = 1, \ldots, 8$) is

$$f_i = \begin{cases} \dfrac{w_i s_i^M}{\sum_{j=1}^{8} \left(\max\{0, w_j s_j\}\right)^M} & \text{for } s_i > 0\,, \\ 0 & \text{for } s_i < 0\,, \end{cases} \tag{1}$$

where s_i is the slope gradient which is defined positive for downward slopes. Higher values of flow-exponent M results in more convergent flow. This algorithm reduces to standard FD8 when $M = 1$ while D8 behaviour is obtained at limit $M \to \infty$.

In Equation 1, each direction was weighed by coefficient w_i which can be different for cardinal and diagonal directions. We set the weights for diagonal directions to unity and for cardinal directions we use adjustable parameter W. Note, that only the ratio of cardinal and diagonal weights is essential due to the normalization in Equation 1. Quinn *et al*. (1991) used a simple geometric construction to select $W = 1.4124$, and also value $W = 1$ is regularly used. In the following, W is used as an adjustable parameter to improve the rotational invariance of flow routing.

2.2. *Flow accumulation*

Flow accumulation (also known as upslope contributing area) is an important quantity to many hydrologic models utilizing DEMs. To compute flow accumulation, we assume that each grid cell initially has one unit of water. In addition, it is assumed that the terrain surface is impermeable and that no evaporation occurs. Flow accumulation computations rely on the flow fractions given by the selected flow routing algorithm. In flow accumulation computation, the amount of water flowing from the upslope cells through a given grid cell is determined. In other

words, the flow accumulation calculates the area that produces run-off to a grid cell. The flow accumulation process can perhaps easiest be described with the help of recursive algorithm (Tarboton 1997). Flow accumulation of a grid point equals to its own water unit plus the fractions of the flow accumulations of the upslope cells as determined by the used flow routing algorithm. If the flow accumulation in an upslope cell is not yet determined, the flow accumulation computation in that cell is recursively initiated. For practical computations, more efficient algorithms have been developed including flow transfer, dependency transfer, indegree-based and topological-sort-based algorithms (Ortega and Rueda 2010, Qin and Zhan 2012, Sten *et al*. 2016).

2.3. *Analysis method*

The rotational invariance of the calculated flow accumulation results are analysed and quantified with the method described in the following.

First we define rotation matrix as

$$R_\theta = \begin{pmatrix} \cos\theta & -\sin\theta \\ \sin\theta & \cos\theta \end{pmatrix}. \tag{2}$$

This matrix rotates the points in two-dimensional Cartesian coordinate system about the origin through angle θ. The inverse rotation is

$$R_\theta^{-1} = R_{-\theta} = \begin{pmatrix} \cos\theta & \sin\theta \\ -\sin\theta & \cos\theta \end{pmatrix}. \tag{3}$$

The analysis starts with the original DEM of size $N_x \times N_y$. A rotated version of the original DEM is obtained by rotating the grid about its centre point and interpolating new elevation values. Rotated DEM is stored in a grid of size $M_x \times M_y$, which is large enough so that the rotated DEM fits to the new grid. Let $\mathbf{r}' = (i,j)^T$ be a grid node (with q grid indices i and j) in the rotated DEM. Coordinates of this point in the original coordinate system are

$$\mathbf{r} = R_\theta^{-1}(\mathbf{r}' - \mathbf{R}') + \mathbf{R}, \tag{4}$$

where $\mathbf{R} = 0.5(N_x + 1, N_y + 1)^T$ and $\mathbf{R}' = 0.5(M_x + 1, M_y + 1)^T$ are the centre points of the original and rotated grids, respectively. While $\mathbf{r}'$ is a grid node in the rotated grid, point $\boldsymbol{r}$ generally does not hit a grid node in the original coordinate system. If $\boldsymbol{r}$ is located between grid nodes an interpolation scheme is needed. The elevation value in the rotated grid is interpolated from the four neighbouring grid nodes using bilinear interpolation scheme. Interpolated elevation value is obtained as

$$z'(\mathbf{r}) = \sum_{\mathbf{X}} z(\mathbf{X})\delta_{\Delta x}(\mathbf{r} - \mathbf{X})\Delta x^2, \tag{5}$$

where summation runs over all grid nodes $\boldsymbol{X}$ in the original grid, Δx is the grid spacing and $\delta_{\Delta x}$ is a discrete version of the Dirac delta function given by

$$\delta_{\Delta x}(\mathbf{r}) = \frac{1}{\Delta x^2}\phi\left(\frac{x}{\Delta x}\right)\phi\left(\frac{y}{\Delta x}\right). \tag{6}$$

The interpolation stencil reads as

$$\phi(a) = \begin{cases} 1 - |a| & \text{for } 0 \leq |a| \leq 1\,, \\ 0 & \text{for } |a| > 1\,. \end{cases} \tag{7}$$

After solving the elevation values in the rotated grid, flow accumulation is computed for this grid. Thereafter, the resulting flow accumulation grid is subjected to an inverse rotation and flow accumulation values in the nodes of the original grid are calculated by using similar bilinear interpolation that was employed earlier for the elevations. We thus end up with a flow accumulation map that is calculated by using a grid rotated through angle θ but with accumulation values given in the nodes of the original grid. Thus, the flow accumulation maps obtained by using original and rotated grid orientations can be straightforwardly compared.

The flow accumulation grid computed using the rotated DEM was compared to the original one by calculating cross-correlation coefficient. Cross correlation for flow-accumulation grids k and l is obtained as

$$C_{k,l} = \frac{1}{N\sigma_k\sigma_l}\sum_{x,y}(A_k(x,y) - \bar{A}_k)(A_l(x,y) - \bar{A}_l), \tag{8}$$

where N is the number of cells and $A_k(x,y)$ the flow accumulation value (see Section 2.2) of cell at location (x,y) for grid k. σ_k and $\bar{A}_k$ are the standard deviation and average flow accumulation for grid k, respectively. Cross-correlation coefficient varies between values −1 and +1. Cross correlation close to +1 indicating strong correlation between the grids, values around zero indicate that there is no correlation, and values close to −1 imply that one image is almost a 'negative image' of another.

2.4. *Digital elevation models*

Both artificial and real terrains are used as test DEMs. DEMs are divided into two data sets. First dataset (DS1) consists of two artificial and two real terrains, and most of the presented results are obtained by using these DEMs. Second data set (DS2) consists of four real-world DEMs, which serve as additional test cases. DEMs in DS1 and DS2 are visualized in Figures 1 and 2, respectively, where also abbreviations used in the subsequent text are introduced.

First artificial DEM is a cone-shaped hill with slope angle $\alpha = 5^\circ$ given by equation

$$z_{ij} = z_0 + \Delta x\sqrt{(i - x_0)^2 + (j - y_0)^2}\tan\alpha. \tag{9}$$

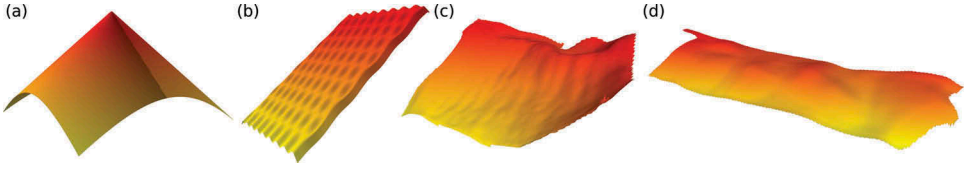

Figure 1. Visualizations of the DEMs in DS1: (a) artificial cone-shaped hill (hereafter Hill), (b) undulating slope (Slope), (c) first field parcel (DEM-A) and (d) second field parcel (DEM-B). In all cases, the elevation values are exaggerated by a factor of 10 to emphasize the small changes in the surface topography.

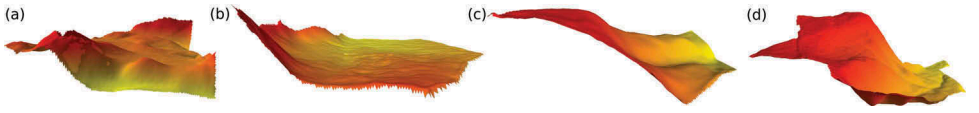

Figure 2. Visualizations of the four real-world DEMs (field parcels) in DS2: (a) DEM-C (b) DEM-D, (c) DEM-E and (d) DEM-D. Elevation values are scaled as in Figure 1.

The size of the DEM is 200×200, the position of the hill top $(x_0, y_0) = (100.5, 100.5)$ and the grid spacing $\Delta x = 2$ m (Figure 1(a)).

Second artificial DEM is an undulating slope given by equation

$$z_{ij} = z_0 + \Delta x i \tan\alpha + A \sin\left(\frac{2\pi i}{\lambda_x}\right) \sin\left(\frac{2\pi j}{\lambda_y}\right). \tag{10}$$

The average slope angle is $\alpha = 5°$, amplitude $A = 0.5$ m, and wave lengths $\lambda_x = 45$ and $\lambda_y = 25$. Also here the grid spacing is $\Delta x = 2$ m. These parameter values ensure that the surface does not have local depressions. The size of the DEM is 220×200 cells, including a 10-cell-wide downward sloping layer surrounding the actual terrain (see Figure 1(b)). To test the effect of grid spacing on the results, also finer resolutions (with grid spacings 0.2, 0.5 and 1 m) are used for this surface.

Six field parcels located in southern Finland are used as real-world DEMs. Two DEMs in DS1 are shown in Figure 1(c,d), and four DEMs in DS2 in Figure 2. These DEMs are based on airborne LIDAR scanning and retrieved from National Land Survey of Finland, and their horizontal resolution is 2 m. Areas of the field parcels are 4.4 ha (DEM-A), 8.4 ha (DEM-B), 8.8 ha (DEM-C), 15.5 ha (DEM-D), 4.1 ha (DEM-E) and 23.8 ha (DEM-F).

2.5. *Simulation set-up*

All simulations reported in the next section followed similar procedure. After selecting the test DEM, flow accumulation map was calculated using the original grid and the selected values for M and W in flow routing (Equation 1). Then the grid was rotated through angle θ and flow accumulation was determined for the rotated DEM using same parameter values. The obtained flow accumulation map was then rotated to the original coordinate system and the obtained map was compared to that computed for the original DEM via cross-correlation analysis. A graphical representation of the numerical experiments is shown in Figure 3.

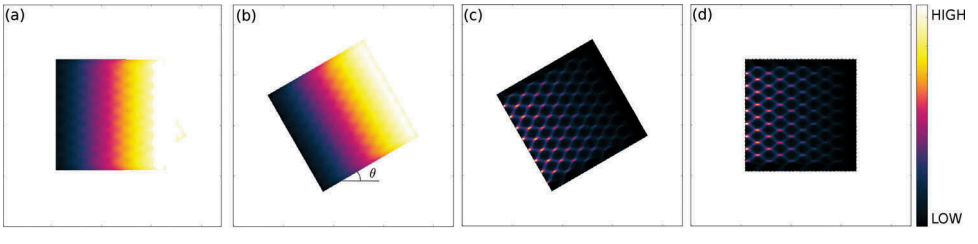

Figure 3. Rotation procedure. From left to right: (a) original DEM (slope DEM is used here as example), (b) DEM rotated through angle θ, (c) flow accumulation map computed for rotated DEM, (d) flow accumulation map after inverse rotation. Cross correlation is calculated for the flow accumulation map determined for original grid and the map shown in panel (d).

3. Results

Flow accumulation maps calculated for the artificial Hill DEM are shown in Figure 4. The results that were obtained by selecting flow exponent $M = 3$ and weight $W = 1$ (upper panels (a,b)) appear highly anisotopic although the used DEM had perfect rotational symmetry. In spite of this, cardinal and diagonal directions have clearly deviating behaviour whereby the observed flow accumulation pattern has a clear dependence on the grid orientation and patterns obtained for original and rotated ($\theta = 40°$) DEMs are evidently different.

Rotational invariance can be significantly improved by adjusting parameter W. As shown in Figure 4 (lower panels (c,d)), by setting $W = 3.5$ the flow accumulation pattern has practically perfect rotational symmetry, and the obtained result is independent of the grid orientation. Therefore also the results obtained for original and rotated grid are practically identical.

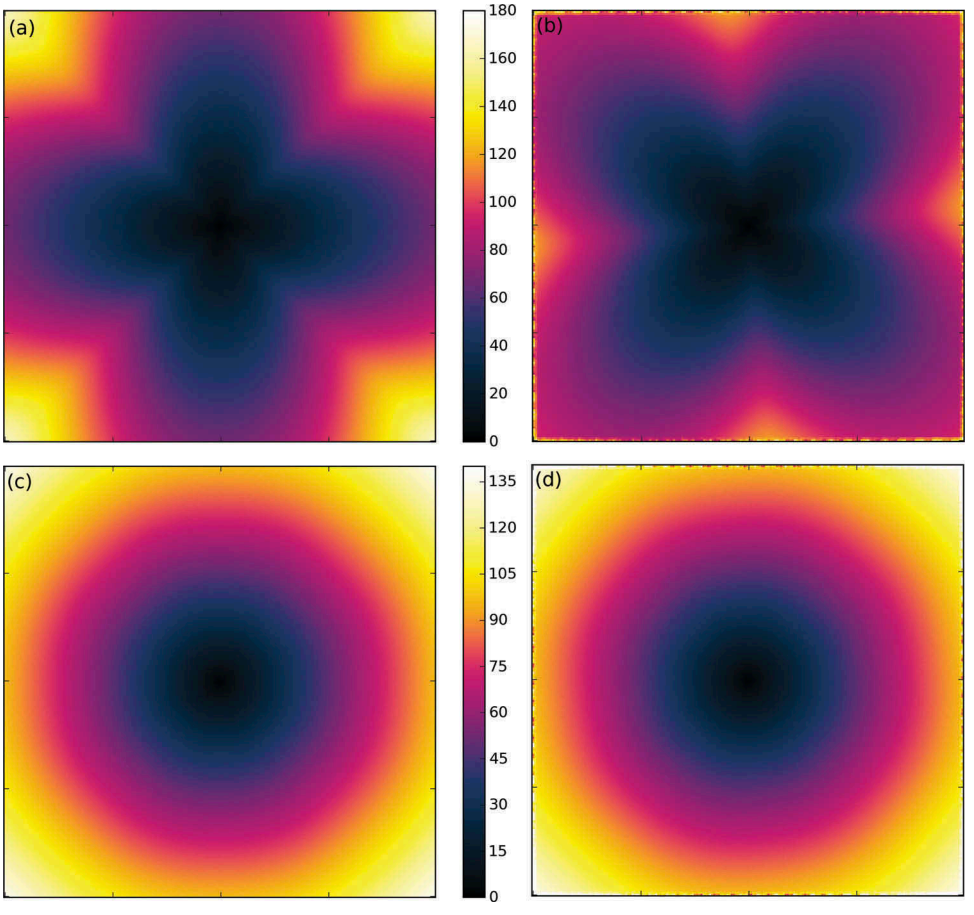

Figure 4. Flow accumulation patterns obtained for Hill DEM. The used flow exponent was $M = 3$ in all cases and the weight W was 1 (upper panels, a and b) or 3.5 (lower panels, c and d). On the left shown are the results obtained for DEM with original grid orientation and on the right results for DEM rotated 40°.

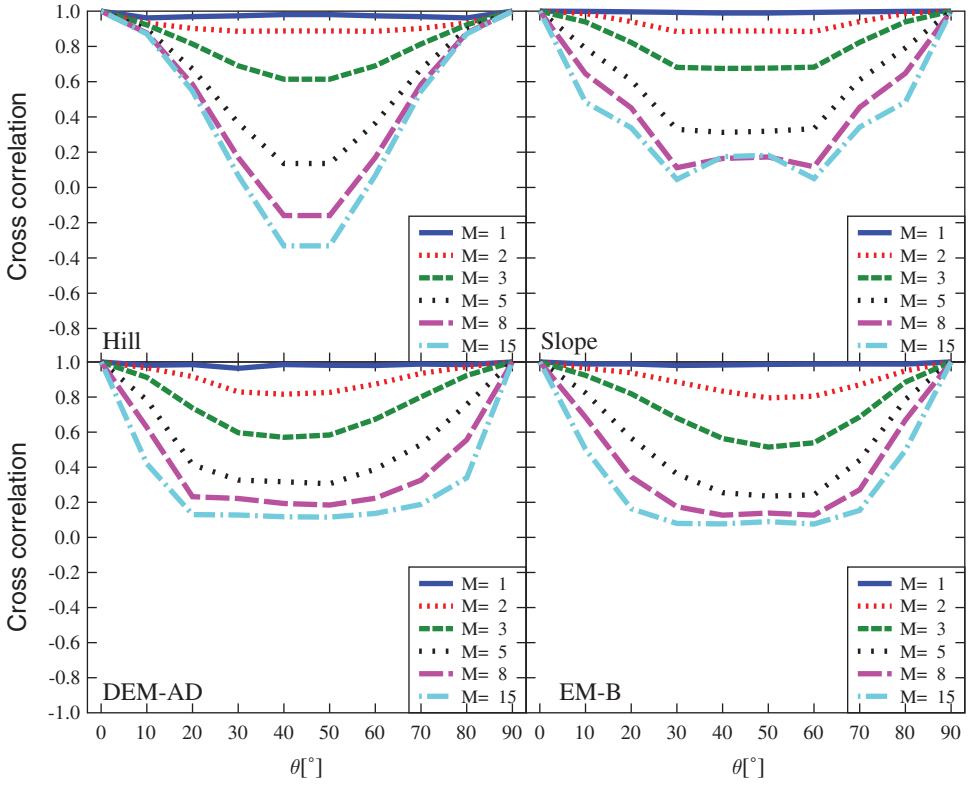

Figure 5. Cross correlations between the flow accumulations computed for rotated and original grid. Results are shown for all four tested DEMs and six flow exponents for each DEM. weight factor $W = 1$.

In Figure 5 the cross correlations for the original DEMs and rotated DEMs ($\theta = 0°, 10°, \ldots, 90°$) are shown. Cross correlations were calculated for DEMs in DS1 using six flow exponents in range from 1 to 15. In these computations, weight W was set to unity. We observe that cross correlations are close to 1 when $M = 1$, i.e. for the FD8 method, but that rotational invariance weakens with increasing M. Especially when $\theta \approx 45°$, cross correlations can be close to 0 for large flow exponent. Even negative cross correlations were observed for the Hill DEM when setting $M = 8$ or $M = 15$. Another observation is that for more complex land surface (Slope, DEM-A, DEM-B), greater decreases in the cross correlation are observed even for small rotation angles.

Next we consider how weight factor W can be utilized to minimize the grid orientation dependence. In Figure 6, cross correlation as a function of W is shown for DEMs in DS1. In this test, cross correlation between the original grid and grid rotated by 30° was calculated. We observe that performance of the flow routing algorithms can be considerably improved by careful selection of W. Even though the performance of flow routing is reasonably good for FD8 with $M = 1$, the situation can be further improved by fine tuning. For higher values of M, the improvement can be more remarkable. However, the cross correlation value obtained by using optimal W decreases as the flow exponent

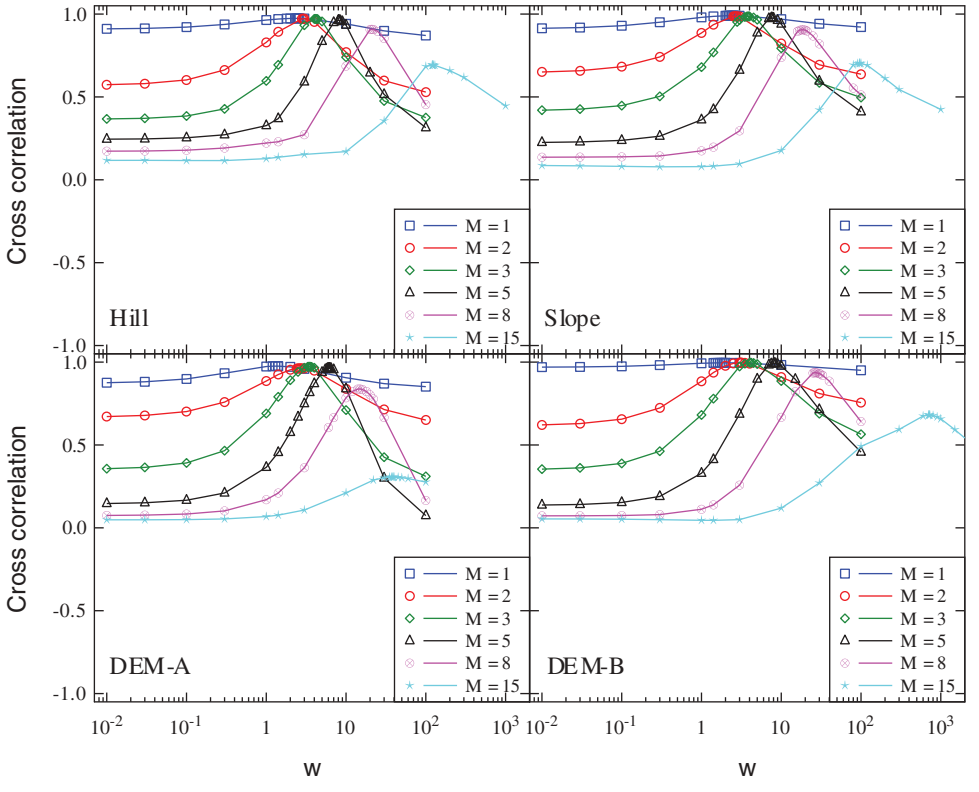

Figure 6. Cross correlation between flow accumulations computed using original and rotated (30°) grids. Weight factor W was varied to find the optimal W for each DEM.

increases. The situation is quite good up to $M = 5$ but when the flow routing method approaches SFD behaviour (cases $M = 8$ and $M = 15$), grid orientation dependence becomes more apparent. General trend is that optimal value of W increases with increasing M.

The optimal W values are shown in Table 1 for all tested DEMs including those in DS2. We notice that the optimal weight is DEM dependent. Most deviant results were obtained for the Hill DEM which differs from the other DEMs due to its intrinsic

Table 1. Optimal values of weight W.

	M					
DEM	1	2	3	5	8	15
Hill	1.3	2.7	3.5	6.2	15	38
Slope	2.0	3.1	4.1	8.1	27	710
DEM-A	2.4	2.9	4.1	8.1	21	122
DEM-B	2.5	2.7	3.9	7.6	18	96
DEM-C	2.2	3.0	4.2	8.2	22	177
DEM-D	3.1	2.9	4.0	7.7	20	164
DEM-E	2.9	2.9	3.9	7.9	24	479
DEM-F	2.5	3.0	4.1	8.6	29	700
Mean	2.6	2.9	4.0	8.0	22	290

Artificial DEMs Hill and Slope are omitted from the calculation of mean.

rotational symmetry. For other test DEMs, the optimal values were quite similar. The optimal weight depends on the M value such that higher optimal W values are found for higher M values. The only exception to this rule is found for DEM-D (cases $M = 1$ and $M = 2$).

Next the effect of DEM resolution on the optimal W value is considered. The optimal W value was determined for Slope DEM using three finer grids with grid spacings 0.2, 0.5 and 1 m in addition to the DEM with 2-m grid spacing used above. The same W value that was found optimal for the 2-m DEM produced highest cross correlations also for finer grids.

Finally, we consider the qualitative differences in the flow accumulation patterns determined for terrain DEM-A. In Figure 7, the upper panels show the flow accumulation patterns computed using parameter values $M = 3$ and $W = 1$. Clearly the pattern obtained by using the original grid orientation (a) differs form the one with grid rotated by 30° (b). The situation changes after setting the directional weight to its optimal value $W = 4.1$. The flow accumulation patterns obtained by using the original (c) and rotated (d) grid appear clearly similar.

As a last remark, we note that the two interpolation processes performed in the analysis do not have significant effect on the results. This was confirmed by taking the flow accumulation map computed for the original Slope DEM as a starting point. This map was then subjected for rotation and inverse rotation and the map obtained after these two rotations and related bilinear interpolations was then compared to the flow accumulation map computed using the original DEM without any rotations. For all tested rotation angles ($\theta = 0°, 10°, \ldots, 90°$), obtained cross correlation value was greater than 0.99 indicating that rotations and interpolations have minimal effects on the results.

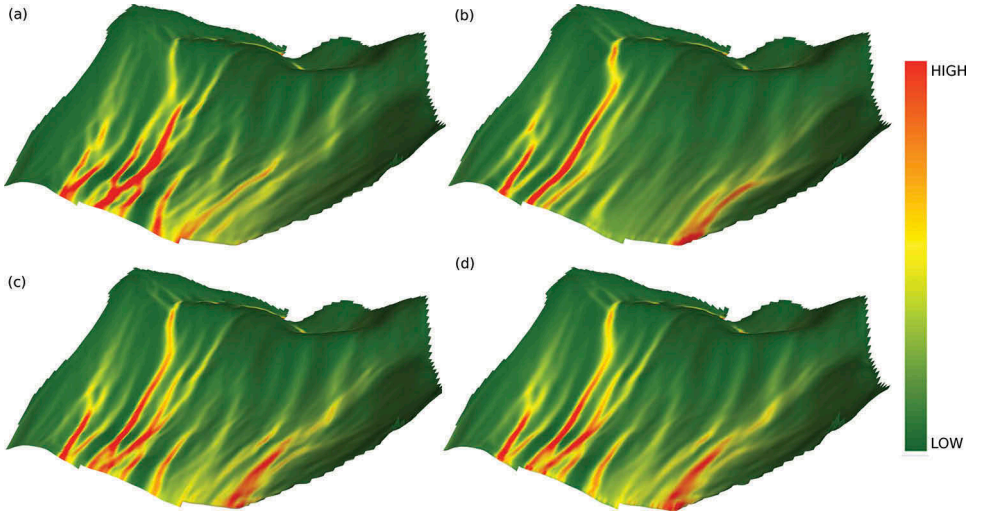

Figure 7. Flow accumulation patterns determined for terrain DEM-A. Left panels are obtained by using the original grid orientation and right panels using grid rotated 30°. Weight factor in (a) and (b) was $W = 1$ and in (c) and (d) $W = 4.1$. In all cases, flow exponent was $M = 3$. Elevation values are scaled as in Figure 1.

4. Discussion

The results presented above indicate that orientation of the computational grid has a considerable impact on the computed flow accumulation patterns. The flow accumulation patterns obtained using Hill DEM are clearly unphysical for $W = 1$ (see Figure 4). Hill DEM has a circular symmetry (surface is similar for any rotation angle about the hilltop), whereby the flow accumulation pattern should possess same symmetry. This is because flow accumulation pattern should be a consequence of the radial flow field given by shallow water equations. In this case, the flow accumulation pattern, however, has a fourfold rotational symmetry which reflects the underlying grid structure. Therefore this unphysical pattern cannot be removed by using finer grid.

This finding means that computations based on flow routing contain discretization errors which result from the insufficient isotropy of the computational grid. It must be noted that these errors are not related to inaccuracies in the elevations or those arising from too large grid cell size (Walker and Willgoose 1999, Erskine *et al*. 2007, O'Neil and Shortridge 2013). After adjusting the value of weight factor *W*, circular symmetry could be achieved even though square grid was still used. This requires that one abandons the geometric interpretation for *W*.

Although the insufficient rotational invariance of the model can cause significant local errors, it does not necessarily lead to similarly drastic global errors in applications where the final result is obtained by integration over the whole DEM, such as calculation of soil loss in USLE-type erosion models (Kinnell 2010). However, even in such cases, it is important to be aware of possible errors as the produced maps are often used for identification of sensitive areas, like erosional hotspots (see, e.g., Ferreira *et al*. 2015) similar to those shown in Figure 7. Prediction of sensitive areas may be inaccurate or even incorrect due to the errors arising from insufficient rotational invariance of the model.

The results obtained by altering the flow exponent *M* indicate that MFD algorithms have better rotational invariance than SFD algorithms. This finding is not surprising if taking into account the characteristics of different algorithms, and it is also in line with analyses of other error types in flow routing (see, e.g., Qin *et al*. 2013).

MFD methods suffer from the numerical dispersion as the flow from a cell is partially routed to all downslope cells. On the other hand, SFD methods cause restrictions to the flow configurations. Tarboton (1997) pointed out that while dispersion is inherent in any method, it would be important to minimize dispersion and to model physical dispersion separately if necessarily. With the weighting scheme introduced here, higher *M* values can be used to minimize the numerical dispersion without compromising the rotational invariance of the model.

In practical simulations, parameter *M* is selected to obtain demanded convergence/divergence for the flow, and *W* to minimize the grid orientation dependence. The optimal *W* increases with increasing *M*. While it would be interesting to find connections between optimal *W* values and terrain properties, in practical, work value optimal for *W* can be easily found numerically for used DEM. By using the average values shown in Table 1 as initial guess, optimal *W* values can be easily determined for studied DEM using the numerical approach presented in this article. While the optimal *W* value depends on properties of used DEM, the values obtained for real-world DEMs appear

quite consistent for $M \approx 2-5$. Therefore, it is possible that average values for the real-world DEMs shown in Table 1 can be used more generally.

For highest tested M values, which produce nearly SFD behaviour, the optimal W were found to be remarkably high. In practice, this means that flow routing moves towards a scheme using von Neumann neighbourhood instead of Moore neighbourhood. As a consequence, the rotational invariance remains unsatisfactory even for optimal W.

One possibility to further improve the scheme and generally the rotational invariance of flow routing on square grids could be to use extended neighbourhoods instead of Moore neighbourhood. Extended neighbourhood would increase the number of weight factors in the model. However, while this would provide more possibilities for model tuning, it would also complicate the model. Also, the physical interpretation of the flow accumulation process would become more complicated as well as implementation of such an algorithm.

5. Conclusions

Insufficient rotational invariance may have significant effects on the computations relying on flow routing. Here, a systematic approach for analysing and quantifying the rotational invariance of DEM-based modelling was presented. Numerical experiments were conducted to demonstrate that rotational invariance of flow accumulation maps can be considerably improved by introducing different weight factors for cardinal and diagonal directions in flow routing. This requires that geometrically specified 'contour length' concept that is often used in flow routing is replaced with a new parameter that has purely numerical interpretation. The introduced weight factor has strong dependence on the flow routing model as well as on the properties of used DEM. Further research is needed to find out how terrain characteristics affect the optimal value of W parameter.

Disclosure statement

No potential conflict of interest was reported by the author.

ORCID

Jari Hyväluoma http://orcid.org/0000-0003-1113-439X

References

Beven, K.J. and Kirkby, M.J., 1979. A physically based, variable contributing area model of basin hydrology. *Hydrological Sciences Bulletin*, 24, 43–69. doi:10.1080/02626667909491834

Costa-Cabral, M.C. and Burges, S.J., 1994. Digital Elevation Model Networks (DEMON): a model of flow over hillslopes for computation of contributing and dispersal areas. *Water Resource Research*, 30, 1681–1692. doi:10.1029/93WR03512

de Sousa, L., *et al*., 2006. Assessing the accuracy of hexagonal versus square tilled grids in preserving DEM surface flow directions. *In*: M. Caetano and M. Painho, eds. *7th international symposium on spatial accuracy assessment in natural resources and environmental science 5-7 July 2006*. Lisbon: International Spatial Accuracy Research Association, 191–200.

Erskine, R.H., *et al*., 2007. Digital elevation accuracy and grid cell size: effects on estimated terrain attributes. *Soil Science Society of America Journal*, 71, 1371–1380. doi:10.2136/sssaj2005.0142

Fairfield, J. and Leymarie, P., 1991. Drainage networks from grid digital elevation models. *Water Resources Research*, 27, 709–717. doi:10.1029/90WR02658

Ferreira, V., *et al*., 2015. Predicting soil erosion after land use changes for irrigating agriculture in a large reservoir of southern Portugal. *Agriculture and Agricultural Science Procedia*, 4, 40–49. doi:10.1016/j.aaspro.2015.03.006

Freeman, T.G., 1991. Calculating catchment area with divergent flow based on a regular grid. *Computers & Geosciences*, 17, 413–422. doi:10.1016/0098-3004(91)90048-I

Frisch, U., Hasslacher, B., and Pomeau, Y., 1986. Lattice-gas automata for the Navier-Stokes equation. *Physical Review Letters*, 56, 1505–1508. doi:10.1103/PhysRevLett.56.1505

Garbrecht, J. and Martz, L.W., 1997. The assignment of drainage direction over flat surfaces in raster digital elevation models. *Journal of Hydrology*, 193, 204–213. doi:10.1016/S0022-1694(96)03138-1

Grimaldi, S., *et al*., 2007. A physically-based method for removing pits in digital elevation models. *Advances in Water Resources*, 30, 2151–2158. doi:10.1016/j.advwatres.2006.11.016

Hengl, T. and Reuter, H.I., eds., 2008. Geomorphometry: concepts, software, applications. *In*: *Developments in soil science*. Amsterdam: Elsevier, 33.

Holmgren, P., 1994. Multiple flow direction algorithms for runoff modelling in grid based elevation models: an empirical evaluation. *Hydrological Processes*, 8, 327–334. doi:10.1002/(ISSN)1099-1085

Jenson, S.K. and Domingue, J.O., 1988. Extracting topographic structure from digital elevation models. *Photogrammetric Engineering and Remote Sensing*, 54, 1593–1600.

Kinnell, P.I.A., 2010. Event soil loss, runoff and the universal soil loss equation family of models: a review. *Journal of Hydrology*, 385, 384–397. doi:10.1016/j.jhydrol.2010.01.024

Lea, N.L., 1994. An aspect driven kinematic routing algorithm. *In*: A.J. Parsons and A.D. Abrahams, eds. *Overland flow: hydraulics and erosion mechanics*. New York: Chapman & Hall, 147–175.

Nardi, F., *et al*., 2008. Hydrogeomorphic properties of simulated drainage patterns using digital elevation models: the flat area issue. *Hydrological Sciences Journal*, 53, 1176–1190. doi:10.1623/hysj.53.6.1176

O'Callaghan, J.F. and Mark, D.M., 1984. The extraction of drainage networks from digital elevation data. *Computer Vision, Graphics, and Image Processing*, 28, 323–344. doi:10.1016/S0734-189X(84)80011-0

O'Neil, G. and Shortridge, A., 2013. Quantifying local flow direction uncertainty. *International Journal of Geographical Information Science*, 27, 1292–1311. doi:10.1080/13658816.2012.719627

Ortega, L. and Rueda, A., 2010. Parallel drainage network computation on CUDA. *Computers & Geosciences*, 36, 171–178. doi:10.1016/j.cageo.2009.07.005

Qin, C., *et al*., 2013. Artificial surfaces simulating complex terrain types for evaluating grid-based flow direction algorithms. *International Journal of Geographical Information Science*, 27, 1055–1072. doi:10.1080/13658816.2012.737920

Qin, C., *et al*., 2007. An adaptive approach to selecting a flow-partition exponent for a multiple-flow-direction algorithm. *International Journal of Geographical Information Science*, 21, 443–458. doi:10.1080/13658810601073240

Qin, C.-Z. and Zhan, L., 2012. Parallelizing flow-accumulation calculations on graphics processing units - From iterative DEM preprocessing algorithm to recursive multiple-flow-direction algorithm. *Computers & Geosciences*, 43, 7–16. doi:10.1016/j.cageo.2012.02.022

Quinn, P., *et al*., 1991. The prediction of hillslope flow paths for distributed hydrological modelling using digital terrain models. *Hydrological Processes*, 5, 59–79. doi:10.1002/(ISSN)1099-1085

Sørensen, R. and Seibert, J., 2007. Effects of DEM resolution on the calculation of topographical indices: TWI and its components. *Journal of Hydrology*, 347, 79–89. doi:10.1016/j.jhydrol.2007.09.001

Sten, J., *et al*., 2016. Parallel flow accumulation algorithms for graphical processing units with application to RUSLE model. *Computers & Geosciences*, 89, 88–95. doi:10.1016/j.cageo.2016.01.006

Tarboton, D.G., 1997. A new method for the determination of flow directions and upslope areas in grid digital elevation models. *Water Resources Research*, 33, 309–319. doi:10.1029/96WR03137

Walker, J.P. and Willgoose, G.R., 1999. On the effect of digital elevation model accuracy on hydrology and geomorphology. *Water Resources Research*, 35, 2259–2268. doi:10.1029/1999WR900034

Wilson, J., 2012. Digital terrain modeling. *Geomorphology*, 137, 107–121. doi:10.1016/j.geomorph.2011.03.012

Wilson, J.P., *et al*., 2008. Water in the landscape: a review of contemporary flow routing algorithms. *In*: Q. Zhou, B. Lees, and G. Tang, eds. *Advances in digital terrain analysis*. New York: Springer, 213–236.

Wilson, J.P., Lam, C.S., and Deng, Y., 2007. Comparison of the performance of flow routing algorithms used in GIS-based hydrologic analysis. *Hydrological Processes*, 21, 1026–1044. doi:10.1002/(ISSN)1099-1085

Wolock, D.M. and Price, C.V., 1994. Effects of digital elevation model map scale and data resolution on a topography-based watershed model. *Water Resources Research*, 30, 3041–3052. doi:10.1029/94WR01971

Zhou, Q. and Liu, X., 2002. Error assessment of grid-based flow routing algorithms used in hydrological models. *International Journal of Geographical Information Science*, 16, 819–842. doi:10.1080/13658810210149425

Zhou, Q. and Liu, X., 2004. Analysis of errors of derived slope and aspect related to DEM data properties. *Computers & Geosciences*, 30, 369–378. doi:10.1016/j.cageo.2003.07.005